Frontiers of Information Technology & Electronic Engineering
www.jzus.zju.edu.cn; engineering.cae.cn; www.springerlink.com
ISSN 2095-9184 (print); ISSN 2095-9230 (online)
E-mail: jzus@zju.edu.cn

Assembly variation analysis of flexible curved surfaces based on Bézier curves*

Zhen-yu LIU, Shi-en ZHOU, Jin CHENG†‡, Chan QIU, Jian-rong TAN

State Key Lab of CAD & CG, Zhejiang University, Hangzhou 310027, China

†E-mail: cjinpjun@zju.edu.cn

Received Oct. 10, 2016; Revision accepted Jan. 22, 2017; Crosschecked June 8, 2018

Abstract: Assembly variation analysis of parts that have flexible curved surfaces is much more difficult than that of solid bodies, because of structural deformations in the assembly process. Most of the current variation analysis methods either neglect the relationships among feature points on part surfaces or regard the distribution of all feature points as the same. In this study, the problem of flexible curved surface assembly is simplified to the matching of side lines. A methodology based on Bézier curves is proposed to represent the side lines of surfaces. It solves the variation analysis problem of flexible curved surface assembly when considering surface continuity through the relations between control points and data points. The deviations of feature points on side lines are obtained through control point distribution and are then regarded as inputs in commercial finite element analysis software to calculate the final product deformations. Finally, the proposed method is illustrated in two cases of antenna surface assembly.

Key words: Assembly variation analysis; Feature points; Side lines; Flexible curved surfaces; Bézier curves
https://doi.org/10.1631/FITEE.1601619 **CLC number:** TH161+.7

1 Introduction

Flexible curved surface assembly has been widely used in the automotive and aerospace industries (Marciniak et al., 2002). Car structures and aircraft envelopes are made up of a lot of flexible curved surfaces that determine together how the product functions. For example, the aerodynamic body of a vehicle contributes to lower wind resistance, and the smooth surface of an airplane has better electromagnetic antenna performance. When deviations are generated in surface shapes in the manufacturing process, product performance will be influenced. Then assembly variation analysis is needed to calculate the final assembly deformation, which reflects product performance to some extent according to manufacturing deviations. Among assembly variation analysis methods, statistical methods are frequently used to evaluate many surfaces with different deviations to ensure that deviations do not exceed a certain range. Statistical methods of evaluating assembly variations in flexible surfaces are associated with part tolerance zones and assist in product design. Therefore, how to establish a model that can describe these varied surfaces and apply it to assembly variation analysis is significant in predicting the assembly quality.

In general, assembly variation analysis can be divided into two categories: extreme methods and statistical methods (Cai and Qiao, 2011). The former assumes that all parts are in their extreme position (maximum or minimum size). In this case, the assembly deviation is calculated easily, but it is strict and difficult in real-world manufacturing. The most representative statistical method is the Monte Carlo

‡ Corresponding author

* Project supported by the National Natural Science Foundation of China (Nos. 51490663, 51475418, and U1608256) and the National Basic Research Program (973) of China (No. 2015CB058100)

ORCID: Zhen-yu LIU, http://orcid.org/0000-0003-2463-4553

method. A certain number of initial deviations are sampled to calculate the distribution range of the final assembly deviation. The probability of successful assembly can be predicted through virtual assemblies. Compared with extreme methods, statistical methods have advantages in variation analysis. Therefore, the statistical method is applied in this paper.

For traditional variation analysis of rigid parts, the final deviations can be calculated by adding all of part deviations together, because their geometric properties do not change during the process. The variation propagation in the rigid-body assembly process has been discussed by many researchers. Liu et al. (2010) developed a generic state-space approach to model three-dimensional (3D) variation propagation in a multistage assembly process. Yang et al. (2013) considered straight-build assemblies composed of axisymmetric components and proposed a novel variation propagation control method in which individual components are reoriented on a stage-by-stage basis to optimize the table-axis error for the final component in the assembly. Qu et al. (2016) proposed a discrete-time nonlinear state-space model of a mathematical representation for process-oriented locating datum system design. The quantitative relationship between key control characteristics and key product characteristics was established.

However, in flexible surface assembly processes, the linear superposition method is not applied because the shape of parts will change due to the effect of the assembly forces. Methods of discrete feature points and finite element analysis (FEA) have been widely used by researchers to calculate the deformations of part surfaces when performing flexible assembly variation analysis. Liao and Wang (2005a) applied fractal geometry via the Weierstrass-Mandelbrot (W-M) function to model the variation of surface microgeometry of assembly components, and the finite element method was used to analyze the deformation. Lindau et al. (2014) combined the influence coefficient method with a separate detailed subassembly analysis model to facilitate larger flexible assembly structures. Guo et al. (2016) proposed a linear equivalent model using springs, representing the elastic mating surfaces, to calculate variation propagation of 3D assemblies considering geometric variation and part deformation. Based on the 'unit displacement' and 'sensitivity matrix', Gerbino et al. (2008) predicted the final shape variation of multi-station assemblies using statistical variations in key feature points. According to feature functions, Yu and Yang (2015) divided the surface features into four types: basic locating points, additional locating points, measurement points, and welding points. A linear relationship between the input part variations and the output assembly variation was established by variation analysis. Because the welding process in shipbuilding is clearly different from that of the automotive and aerospace industries, Choi and Chung (2015) used welding distortion patterns and a transformation matrix to efficiently model the deformations for variation analysis. In this research of flexible assembly variation analysis, all feature points on surfaces were assumed to be independent of each other in the assembly process to simplify the problem. However, actual surfaces are continuous, and physical relationships among neighboring points on the same surface must be considered. If assuming random variables are independent, the assembly variation will increase as more points with initial errors are considered. In fact, the stiffness of the assembly increases when the number of welding points increases, and the assembly variation may decrease instead. So, it is not adequate to predict the assembly quality if the relationships among points are neglected.

Another simplification problem of existing methods is that distributions of all feature points on flexible curved surface parts are regarded as the same. Camelio et al. (2004) found that the deformations on nodes depend on the geometric relationships among them and part stiffness. A covariance matrix was used to describe the relationships among neighboring points on the same surface to calculate the final deviations. Tonks and Chase (2004) proposed an orthogonal polynomial based covariance model to account for surface variations of the compliant parts over a wide range of wavelengths. A series of Legendre polynomials were used to approximate the actual geometric shape of the plane to model the surface features of parts. Huang et al. (2014) used a discrete cosine transform (DCT) to model part form errors. They decomposed the error fields into a series of independent error modes to represent different kinds of errors in manufacturing processes. The relationship between tolerance expression and

uncertainty factors was established. Liao and Wang (2005b) proposed a new method based on wavelet analysis and the finite element method for variation analysis of nonrigid assemblies. The final assembly deviations were predicted according to part variations in different scales. These methods do not consider the tolerance zones of curved surfaces, which are represented by offsets along the normal direction of points. The distributions of feature points will be more or less different according to their positions. The simplification that all feature points have the same distributions is not suitable.

In this study, a methodology based on Bézier curves is proposed to solve problems of flexible surface assemblies. Through this method, the structure of a curved surface is modeled to represent the part's surface. Compared to traditional flexible variation analysis methods, surface continuity and distributions of different feature points are considered in this study. Surface continuity is considered through the relationships between control points and data points according to Bernstein basis functions, and the distributions of all feature points on side lines are pertinent to the positions of themselves and the control points combined with tolerance constraints.

The proposed method can solve the variation analysis problems mentioned above and it is appropriate to calculate the deformations in flexible surface assemblies. The process of assembly variation analysis is represented by the flow chart in Fig. 1.

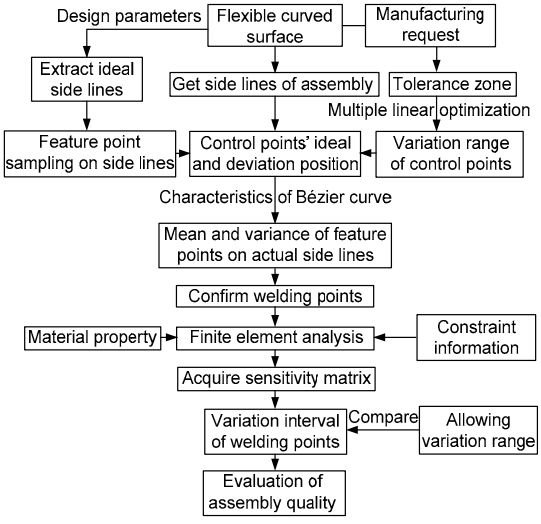

Fig. 1 Flow chart of the proposed method based on Bézier curves

2 Calculating feature point deviations based on Bézier curves

2.1 Representations of flexible curved surface side lines based on Bézier curves

Bézier surfaces can characterize efficiently most curved surfaces because of Bernstein basis functions. These surfaces are suitable for describing the actual flexible curved surface parts for assembly. Its general expression is

$$\boldsymbol{f}(u,v)=\sum_{i=0}^{m}\sum_{j=0}^{n}B_{i,m}(u)B_{j,n}(v)\boldsymbol{P}_{ij}, \tag{1}$$

where u and v are parameters in the interval [0, 1].

As we simplify the assembly process to the matching of two side lines on different parts, it can be expressed by Bézier curves with only one parameter t. If the control points are known as $\boldsymbol{P}_i$ (i=0, 1, …, n) and the Bernstein basis function is $B_i^n(t)$, the side line is an n-order Bézier curve:

$$\begin{cases}\boldsymbol{f}(t)=\sum_{i=0}^{n}B_i^n(t)\boldsymbol{P}_i,\\ B_i^n(t)=\dfrac{n!}{i!(n-i)!}t^i(1-t)^{n-i},\end{cases} \tag{2}$$

where parameter t is a random number within the interval [0, 1].

Bézier curves can be obtained based on the de Casteljau algorithm and represented by geometrical construction. Some points named $\boldsymbol{P}_0$, $\boldsymbol{P}_1$, …, $\boldsymbol{P}_n$ and a one-dimensional scalar t are given. Suppose there is

$$\boldsymbol{P}_i^r(t)=(1-t)\boldsymbol{P}_i^{r-1}(t)+t\boldsymbol{P}_{i+1}^{r-1}(t), \tag{3}$$

where r=1, 2, …, n and i=0, 1, …, $n-r$.

In Eq. (3), $\boldsymbol{P}_i^0(t)$ is equal to $\boldsymbol{P}_i$, and $\boldsymbol{P}_0^n(t)$ is the point on the Bézier curve corresponding to parameter t. The meaning of parameter t can be clearly understood by the partition method:

$$\boldsymbol{P}_i^1=(1-t)\boldsymbol{P}_i+t\boldsymbol{P}_{i+1}, \tag{4}$$

where i=0, 1, …, $n-1$. The geometrical construction of a third-order Bézier curve (n=3) is shown in Fig. 2.

The segment between adjacent control points $\boldsymbol{P}_i$ and $\boldsymbol{P}_{i+1}$ is divided into two parts with the ratio of $t/(1-t)$. This method partition is done time after time, and a Bézier curve will be drawn up when sampling values of t are in the interval [0, 1].

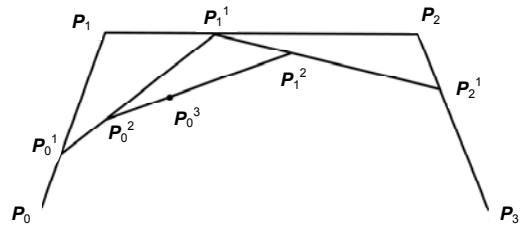

Fig. 2 Geometrical construction of a third-order Bézier curve

2.2 Tolerance zone constraint of flexible curved surface side lines

Compared with a rectangular tolerance zone of a straight-line feature, curved side lines are obtained by making an offset to both sides of Bézier curves along the normal direction of all points. The actual position of the side line is determined by both the normal vector $\boldsymbol{N}(t)$ and the offset value R, where R is a constant and $|R|\leq T/2$. If the tolerance zone is symmetrical to the nominal position and its value is T, the side line after offset can be modeled as

$$\boldsymbol{f}_{\mathrm{R}}(t)=\sum_{i=0}^{n}B_i^n(t)\boldsymbol{P}_i+\frac{R\cdot\boldsymbol{N}(t)}{\sqrt{N(t)_x^2+N(t)_y^2}}, \tag{5}$$

where $N(t)_x^2$ and $N(t)_y^2$ are components of vector $\boldsymbol{N}(t)$ in the x and y directions, respectively.

Generally, variations of feature points on side lines cannot be expressed by an identical pattern. Using control point $\boldsymbol{P}_i$ as a random variable that has a deviation $\boldsymbol{\varepsilon}_i$, a new Bézier curve is obtained. This curve that represents a side line with form errors can be expressed as

$$\begin{aligned}\boldsymbol{f}(t)&=\sum_{i=0}^{n}B_i^n(t)(\boldsymbol{P}_i+\boldsymbol{\varepsilon}_i)\\&=\sum_{i=0}^{n}B_i^n(t)\boldsymbol{P}_i+\sum_{i=0}^{n}B_i^n(t)\boldsymbol{\varepsilon}_i\\&=\boldsymbol{f}_{\mathrm{n}}(t)+\boldsymbol{f}_{\mathrm{e}}(t),\end{aligned} \tag{6}$$

where $\boldsymbol{f}_{\mathrm{n}}(t)$ and $\boldsymbol{f}_{\mathrm{e}}(t)$ are the ideal curve and an error curve, respectively. The deviations of feature points, which are caused by control point variations, vary within a certain range that is decided by the tolerance zone of the side line. So, Eq. (7) can be obtained by combining Eqs. (5) and (6). This indicates that the variation values of feature points on the side line caused by varying of control points must be smaller than half of the tolerance (Fig. 3).

$$\sum_{i=0}^{n}B_i^n(t)\boldsymbol{\varepsilon}_i\leq\frac{T\cdot\boldsymbol{N}(t)}{2\sqrt{N(t)_x^2+N(t)_y^2}}. \tag{7}$$

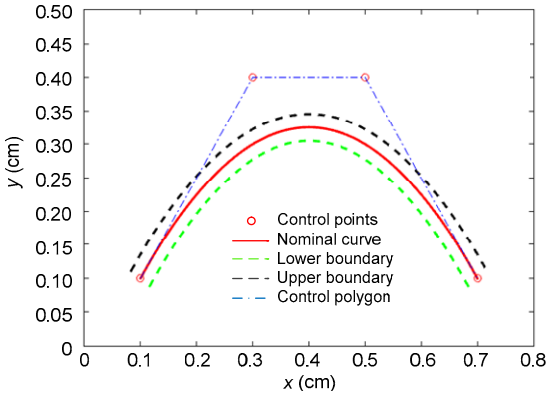

Fig. 3 Nominal position and boundaries of the side line on the curved surface part (References to color refer to the online version of this figure)

2.3 Statistical calculation of side line feature points

2.3.1 Nominal position and deviations of side line control points

According to the analysis mentioned above, determining the control points of flexible curved surface side lines is a precondition for assembly variation analysis. The ideal locations of control points are calculated using the Bernstein basic function, and feature points are sampled on ideal side lines according to design technology.

Suppose that there are m sampling points on the side line, and their coordinates are written into a matrix $\boldsymbol{B}$. $\boldsymbol{B}$ is an $m\times2$ matrix because we consider only points in the two-dimensional space. Note that sampling points must contain starting or ending points of the side line. Based on the Bézier curve, the value of t_1 is 0 at the starting point and the value of t_m is 1 at the ending point. Then $m-1$ segments are obtained by

connecting adjacent sampling points. Their dimensions are calculated through the sampling point coordinates. The k^{th} segment is represented as d_k and k is a positive integer in the interval [1, m–1]. The value of t corresponding to m sampling points can be calculated by the proportion method:

$$\begin{cases} t_1 = 0, \\ t_{k+1} = \dfrac{d_1 + d_2 + \cdots + d_k}{d_1 + d_2 + \cdots + d_{m-1}}, \ k=1, 2, \ldots, m-1. \end{cases} \tag{8}$$

Based on the values of t of m sampling points and the order of Bézier curve n, a Bernstein coefficient matrix $\boldsymbol{M}$ can be determined. For the k^{th} sampling point, its $(i+1)^{\text{th}}$ Bernstein coefficient term is represented by $M_{k,i}$:

$$M_{k,i} = \frac{n!}{i!(n-i)!} t_k^i (1-t_k)^{n-i}. \tag{9}$$

Then the matrix $\boldsymbol{M}$ can be shown as

$$\boldsymbol{M} = \begin{bmatrix} (1-t_1)^n & \cdots & \dfrac{n!}{i!(n-i)!} t_1^i (1-t_1)^{n-i} & \cdots & t_1^n \\ \vdots & & \vdots & & \vdots \\ (1-t_k)^n & \cdots & \dfrac{n!}{i!(n-i)!} t_k^i (1-t_k)^{n-i} & \cdots & t_k^n \\ \vdots & & \vdots & & \vdots \\ (1-t_m)^n & \cdots & \dfrac{n!}{i!(n-i)!} t_m^i (1-t_m)^{n-i} & \cdots & t_m^n \end{bmatrix}_{m\times(n-1)}. \tag{10}$$

We define the matrix of the side line control points as $\boldsymbol{L}$ and it is an $(n+1)\times 2$ matrix. Then the following relationship exists:

$$\boldsymbol{ML} = \boldsymbol{B}. \tag{11}$$

Because $\boldsymbol{M}$ is not a square matrix and cannot be inverted, a matrix $\boldsymbol{M}^{\text{T}}$ is left multiplied to both sides of Eq. (11). A transformation matrix $\boldsymbol{N}$ is defined as $\boldsymbol{N}=\boldsymbol{M}^{\text{T}}\boldsymbol{M}$. Then the matrix of side line control points $\boldsymbol{L}$ is represented as

$$\boldsymbol{L} = \boldsymbol{N}^{-1}\boldsymbol{M}^{\text{T}}\boldsymbol{B}. \tag{12}$$

Nominal control point positions are obtained through Eq. (12) and then we calculate their deviations. Any direction's component of control point deviations is limited by the tolerance components of feature points on side lines in the corresponding direction. Here, a third-order Bézier curve is taken as an example, and the following inequalities exist for any value of t in the interval [0, 1]:

$$\begin{cases} \left|(1-t)^3\varepsilon_{x1} + 3t(1-t)^2\varepsilon_{x2} + 3t^2(1-t)\varepsilon_{x3} + t^3\varepsilon_{x4}\right| \\ \quad \le \dfrac{T}{2}\sin\theta, \\ \left|(1-t)^3\varepsilon_{y1} + 3t(1-t)^2\varepsilon_{y2} + 3t^2(1-t)\varepsilon_{y3} + t^3\varepsilon_{y4}\right| \\ \quad \le \dfrac{T}{2}\cos\theta, \end{cases} \tag{13}$$

where ε_{xi} and ε_{yi} are the i^{th} deviation components of control points in the x and y directions, respectively, T is the tolerance value of a flexible curved surface, and θ ($0\le\theta\le\pi/2$) is the angle between the feature point's normal vector and y direction (Fig. 4). In Eq. (13), the left sides of the inequalities are the third-order expression of t. Through sampling many feature points and constructing a set of inequalities, multiple linear optimization is used to obtain the boundary of the control point's deviation ε.

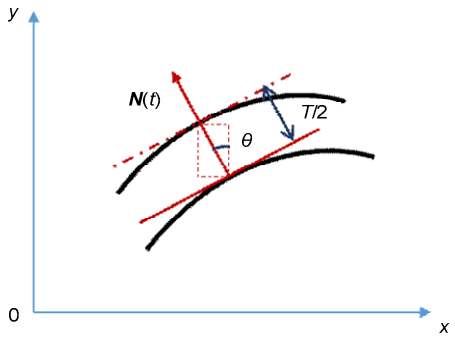

Fig. 4 The nominal position and boundary of side lines on the curved surface part

2.3.2 Probability distribution of side line feature points

Because each component of curve equation $\boldsymbol{f}(t)$ is independent of other components in orthogonal directions, and they have the same Bernstein coefficients, we consider only component $\boldsymbol{f}_y(t)$ in the x-O-y plane. Its matrix can be constructed as

$$\boldsymbol{f}_y(t)=[B_0^n(t)\quad B_1^n(t)\quad\cdots\quad B_n^n(t)]\begin{bmatrix}Y_0\\Y_1\\\vdots\\Y_n\end{bmatrix}=\boldsymbol{B}^n\boldsymbol{P}_Y. \quad (14)$$

The normal distribution is well known in statistics and is often referred to as the Gaussian distribution. In many fields related to a great number of random samples, normal distribution is always more approximate in reality than other distributions. Moreover, the normal distribution is frequently used as an approximation to many other distributions. A popular example is the relationship between the normal and the chi-squared distribution. If x has a standard normal distribution, then x^2 behaves as a chi-squared distribution (Lancaster and Seneta, 2005). In this study, the distributions of control points are considered as normal distributions.

Suppose the mean and variance matrices of control points of the side line are $\boldsymbol{\mu}_{P_Y}$ and $\boldsymbol{\Sigma}_{P_Y}$, respectively. As we know, the mean and variance are the first and second moments of functions, respectively. The mean and variance matrices of every feature point on the side line in the y direction can be obtained through basic statistical methodology:

$$\boldsymbol{\mu}_{y(t)}=E[\boldsymbol{f}_y(t)]=E[\boldsymbol{B}^n\boldsymbol{P}_Y]=\boldsymbol{B}^n\boldsymbol{\mu}_{P_Y}, \quad (15)$$

$$\begin{aligned}\boldsymbol{v}_{y(t)}&=E[(\boldsymbol{f}_y(t)-\boldsymbol{\mu}_{y(t)})\cdot(\boldsymbol{f}_y(t)-\boldsymbol{\mu}_{y(t)})^{\mathrm{T}}]\\&=E[\boldsymbol{B}^n(\boldsymbol{P}_Y-\boldsymbol{\mu}_{P_Y})(\boldsymbol{P}_Y-\boldsymbol{\mu}_{P_Y})^{\mathrm{T}}(\boldsymbol{B}^n)^{\mathrm{T}}]\\&=\boldsymbol{B}^n\boldsymbol{\Sigma}_{P_Y}(\boldsymbol{B}^n)^{\mathrm{T}}.\end{aligned} \quad (16)$$

Due to the special property of Bézier curves, the starting and ending points of side lines and control points are consistent. A coordinate system is built whose x axis is parallel to the line linking these two points and the y axis perpendicular to the x axis. As t is sampled in the interval [0, 1] where t=0 is the starting point and t=1 the ending point, x-axis values of control points are in the interval $[x_0, x_n]$, where x_0 and x_n are the x-axis values of starting and ending points of side lines, respectively. Through Eqs. (15) and (16), the mean and variance of any feature point $\boldsymbol{P}(x_P, y_P)$ on the side line of a flexible curved surface part are obtained. Then a density probability distribution of feature points is obtained in the y direction within the interval $\lfloor\mu_P-3\sqrt{v_P}\,,\ \mu_P+3\sqrt{v_P}\,\rfloor$, where μ_P and v_P are the mean and variance, respectively (Fig. 5).

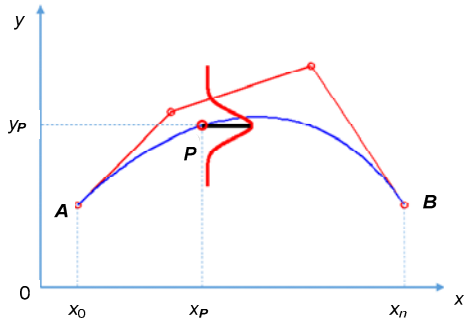

Fig. 5 Mean and variance of a side line on a curved surface part

3 Assembly variation analysis of side lines based on Bézier curves

3.1 Brief description of flexible curved surface assembly

The assembly process of flexible curved surfaces involves many parameters that correlate with one another. It is difficult to describe all variables in the process, so it is essential to make the following assumptions for variation analysis: (1) Part materials are isotropic; (2) Part deformations are in the linear elastic ranges and there is a linear relationship between forces and displacements; (3) The stiffness matrix of parts remains constant and thermal deformations are not considered; (4) The actual and ideal side lines described by Bézier curves have the same order.

In the locating process, two flexible curved surfaces are fixed on the platform using the N-2-1 (N>3) fixture scheme rather than the 3-2-1 scheme, which is used for a rigid body to assure the assembly quality. As shown in Fig. 6, we assume that part 1 has a nominal shape and part 2 has a form error, which is represented by a certain deviation value for the side line. In the clamping process, the initial gap between part 1 and part 2 is forced to be closed by deforming the side line of part 2 to a nominal position. The value of force is the multiplication of the initial deviation and part stiffness. In the welding process, parts 1 and 2 are joined together on the welding points and the gap between them becomes zero. After this process, the two parts will be a product and it has a new

stiffness matrix. In the releasing process, the product composed of parts 1 and 2 will spring back, suffering from the spring-back force with clamps being removed. The value of spring-back variation can be calculated by the force and new stiffness matrix.

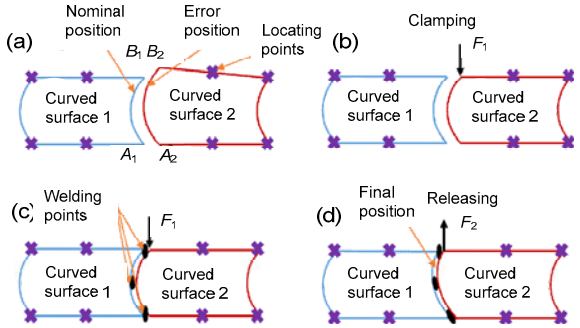

Fig. 6 Four steps of a compliant assembly process: (a) locating process; (b) clamping process; (c) welding process; (d) releasing process

3.2 Calculation of flexible curved surface assembly deformations

FEA is the most popular method for variation analysis of flexible parts. The deviations of all grid nodes can be calculated in this way. In this study, the assembly process of flexible curved surfaces is simplified to the matching of side lines, and the cost of variation analysis is decreased significantly through this simplification. In Section 2.3 we calculated the distributions of all feature points on side lines through control points of Bézier curves. These feature points can be regarded as the inputs of FEA. Then the sensitivity matrix is obtained and we can construct the linear relationship between initial deviations and assembly deviations. Finally, assembly deviations are obtained and the assembly quality is evaluated.

The sensitivity matrix can be obtained in the following way: Suppose two side lines of different flexible curved surface parts both have $N/2$ welding points, where N is a positive even number. Their nominal positions are identical so the welding points follow a one-to-one correspondence. These welding points are on the side lines of flexible curved surfaces and they can be obtained by control points of Bézier curves. Commercial FEA software is used and the specific steps are as follows (Liu and Hu, 1997):

1. A unit force whose direction is the same as the direction of the deviation is applied to the j^{th} (j=1, 2, …, N) source of variation. The first FEA is used to calculate the response of all measurement points. The displacements of nodes are recorded in a column vector $\boldsymbol{C}_j$, which makes up the matrix of influence coefficients. When the system is applied with an arbitrary combination of N forces at source variation points, the relationship between the applied forces $\boldsymbol{F}$ and the displacements of source variation points $\boldsymbol{D}$ can be derived as

$$\boldsymbol{D}=\begin{bmatrix}D_1\\D_2\\\vdots\\D_N\end{bmatrix}=\begin{bmatrix}c_{11}&c_{12}&\cdots&c_{1N}\\c_{21}&c_{22}&\cdots&c_{2N}\\\vdots&\vdots&&\vdots\\c_{N1}&c_{N2}&\cdots&c_{NN}\end{bmatrix}\begin{bmatrix}F_1\\F_2\\\vdots\\F_N\end{bmatrix}=\boldsymbol{CF}. \quad (17)$$

2. In FEA, the stress equation can be written as

$$\boldsymbol{F}=\boldsymbol{KD}=\begin{bmatrix}K_{11}&K_{12}&\cdots&K_{1N}\\K_{21}&K_{22}&\cdots&K_{2N}\\\vdots&\vdots&&\vdots\\K_{N1}&K_{N2}&\cdots&K_{NN}\end{bmatrix}\begin{bmatrix}D_1\\D_2\\\vdots\\D_N\end{bmatrix}. \quad (18)$$

Combined with Eq. (17), the stiffness matrix $\boldsymbol{K}$ can be written as

$$\boldsymbol{K}=\boldsymbol{C}^{-1}, \quad (19)$$

where every column of $\boldsymbol{K}$ is the forces needed from the clamps to produce the unit deviation at the j^{th} source of variation.

3. The second FEA is used to calculate the spring-back displacements at key points in the y direction for the welded structure. s_{ij} (i=1, 2, …, N) is the displacement calculated by FEA at the i^{th} point due to the unit deviation at the j^{th} source of variation. $\boldsymbol{S}$ is the sensitivity matrix and $\boldsymbol{U}$ the total spring-back (assembly variation):

$$\boldsymbol{U}=\begin{bmatrix}S_{11}&S_{12}&\cdots&S_{1N}\\S_{21}&S_{22}&\cdots&S_{2N}\\\vdots&\vdots&&\vdots\\S_{N1}&S_{N2}&\cdots&S_{NN}\end{bmatrix}\begin{bmatrix}D_1\\D_2\\\vdots\\D_N\end{bmatrix}=\boldsymbol{SD}. \quad (20)$$

Based on the mean matrix $\boldsymbol{\mu}_{\boldsymbol{P}_y}$ and variance matrix $\boldsymbol{\Sigma}_{\boldsymbol{P}_y}$ of the side line control points in the y direction, which are calculated in Section 3.1, the mean and

variance matrices of welding points on two parts are $\boldsymbol{B}_1^n\boldsymbol{\mu}_{1,\boldsymbol{P}_y}$, $\boldsymbol{B}_1^n\boldsymbol{\Sigma}_{1,\boldsymbol{P}_y}(\boldsymbol{B}_1^n)^{\mathrm{T}}$, $\boldsymbol{B}_2^n\boldsymbol{\mu}_{2,\boldsymbol{P}_y}$, and $\boldsymbol{B}_2^n\boldsymbol{\Sigma}_{2,\boldsymbol{P}_y}(\boldsymbol{B}_2^n)^{\mathrm{T}}$, respectively. Subscripts 1 and 2 represent the number of assembly parts. After assembly, the mean and variance matrices of welding points are $\boldsymbol{\mu}_a=\boldsymbol{S}\boldsymbol{\mu}_t$ and $\boldsymbol{v}_a=\boldsymbol{S}\boldsymbol{v}_t\boldsymbol{S}^{\mathrm{T}}$, respectively. $\boldsymbol{\mu}_t$ and $\boldsymbol{v}_t$ are derived as

$$\boldsymbol{\mu}_t=\begin{bmatrix}\boldsymbol{B}_1^n(t_1)\boldsymbol{\mu}_{1,\boldsymbol{P}_y}\\ \vdots\\ \boldsymbol{B}_1^n(t_{N/2})\boldsymbol{\mu}_{1,\boldsymbol{P}_y}\\ \boldsymbol{B}_2^n(t_1)\boldsymbol{\mu}_{2,\boldsymbol{P}_y}\\ \vdots\\ \boldsymbol{B}_2^n(t_{N/2})\boldsymbol{\mu}_{2,\boldsymbol{P}_y}\end{bmatrix}, \tag{21}$$

$$\boldsymbol{v}_t=\begin{bmatrix}\boldsymbol{B}_1^n(t_1)\cdot\boldsymbol{\Sigma}_{1,\boldsymbol{P}_y}\cdot(\boldsymbol{B}_1^n(t_1))^{\mathrm{T}}\\ \vdots\\ \boldsymbol{B}_1^n(t_{N/2})\cdot\boldsymbol{\Sigma}_{1,\boldsymbol{P}_y}\cdot(\boldsymbol{B}_1^n(t_{N/2}))^{\mathrm{T}}\\ \boldsymbol{B}_2^n(t_1)\cdot\boldsymbol{\Sigma}_{2,\boldsymbol{P}_y}\cdot(\boldsymbol{B}_2^n(t_1))^{\mathrm{T}}\\ \vdots\\ \boldsymbol{B}_2^n(t_{N/2})\cdot\boldsymbol{\Sigma}_{2,\boldsymbol{P}_y}\cdot(\boldsymbol{B}_2^n(t_{N/2}))^{\mathrm{T}}\end{bmatrix}. \tag{22}$$

The clearance between the actual position and nominal position of welding points is regarded as the key characteristic parameter. An actual welding line, which is in a confidence interval, is obtained according to the mean and variance matrices of welding points. As shown in Fig. 7, the blue area represents confidence interval $\lfloor\mu_{\boldsymbol{P}}-3\sqrt{v_{\boldsymbol{P}}}\,,\ \mu_{\boldsymbol{P}}+3\sqrt{v_{\boldsymbol{P}}}\,\rfloor$, and the final position of the welding line will fall within this range with a probability of 99.7%.

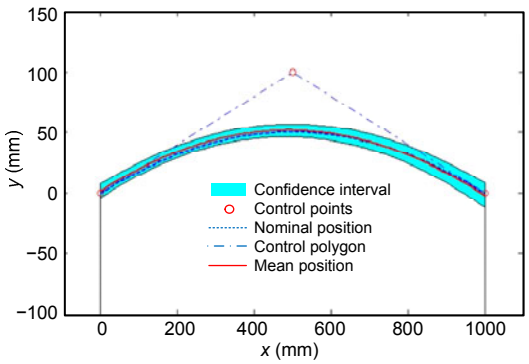

Fig. 7 Nominal position and confidence interval of the welding line (References to color refer to the online version of this figure)

4 Case study

In assemblies of flexible surfaces like antennas, surface continuity and distributions of feature points must be considered because their functions are hypersensitive to structure deformations. Deviations of antenna surfaces need to be small enough to satisfy the product performance. Such deviation units are always at the millimeter or even the micron level. Research has shown that a small difference will cause violent changes in the antenna function. The root mean square (RMS) surface deformations are modeled as intervals to calculate their influence on reflector antenna energy by Rocca et al. (2014). Chaumette (2006) analyzed a conformal antenna array fitted to the surface of a nonplanar part of modern aircrafts to prove that the occurrence of static and dynamic deformations had a severe impact on the performance of conformal antennas.

In this section, the proposed method is illustrated using two cases of antenna surface assemblies. The deviations of key points on side lines of the antenna surfaces are calculated precisely to ensure performance.

4.1 Reflector antenna surface assembly

An example of reflector antenna surface assembly is shown in Fig. 8. According to the four-step assembly of flexible curved surfaces and the method of variation analysis based on Bézier curves in Section 2, FEA is done in commercial analysis software. The sensitivity matrix is obtained and final assembly deviations on welding line of the reflector antenna are calculated.

Usually the order n of Bézier curves describing side lines is not greater than 3. Here, we set n=3 as reflector antennas often have regular shapes. The connecting direction of the side line's starting and ending points is treated as the x axis to build the coordinate system. A set of feature points on the side line are sampled (Fig. 9), and part of their coordinates are (0, 0), (33.925, 5.044), (70.611, 8.014), (114.356, 8.069), (152.096, 4.96), and (183.848, 0). The coordinate units are centimeters and four control point coordinates of this side line are calculated according to Section 2.3 as $\boldsymbol{A}$(0, 0), $\boldsymbol{B}$(70.13, 12.67), $\boldsymbol{C}$(131.5, 9.987), and $\boldsymbol{D}$(183.848, 0).

In the design stage, the manufacturing tolerance

of the reflector antenna is set as 0.65 cm and its upper and lower deviations are +0.45 cm and −0.20 cm, respectively. Based on the equations mentioned in Section 2.3, the boundaries of four control points are obtained according to the number of sampling points on the side line. Their limits are [−0.098, 0.392], [−0.216, 0.45], [−0.228, 0.432], [−0.098, 0.392] (in centimeters) in turn. These control points of the reflector antenna's side line have deviations from ideal positions in the y direction and all of them are supposed to follow a normal distribution. Their mean and variance values are shown in Table 1.

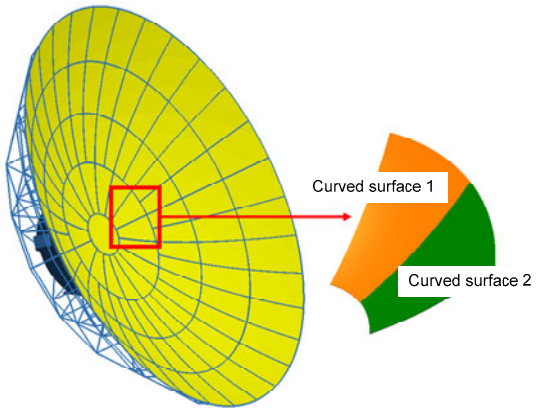

Fig. 8 Assembly of two parts of a reflector antenna

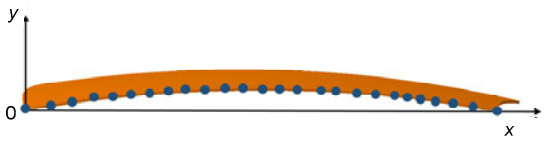

Fig. 9 Sampling points of the reflector antenna's side line

According to the method proposed in Section 2, the feature points on the side line are calculated. Their mean and variance are calculated through the value of t, which is in the interval [0, 1] (Eq. (23)). The positions of control points and the actual shape of the reflector antenna's side line are illustrated in Fig. 10.

$$\begin{cases} \mu_t = 0.147(1-t)^3 + 0.351t^2(1-t) + 0.147t^3, \\ v_t = 0.0067(1-t)^6 + 0.1107t^2(1-t)^4 \\ \quad + 0.1089t^4(1-t)^2 + 0.0067t^6. \end{cases} \tag{23}$$

Based on the projection of feature points on the side lines to the x axis, 11 welding points are obtained according to uniform sampling. Their mean and variance values in the y direction before assembly are shown in Table 2, as well as their corresponding x values and t values in the Bernstein basis function.

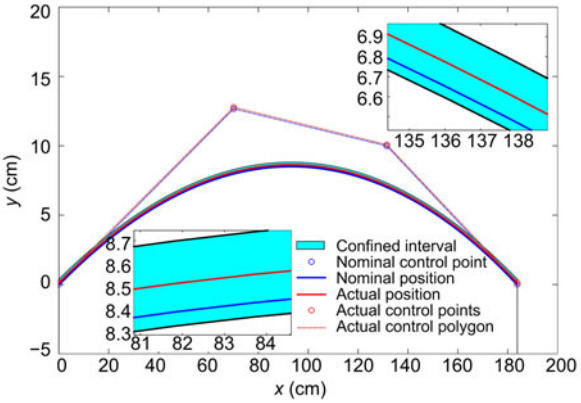

Fig. 10 Mean and variance distributions of feature points on the side line of the reflector antenna (References to color refer to the online version of this figure)

Table 1 Mean and variance of the reflector antenna's control points on the side line

Control point	Mean (cm)	Variance (cm)
A	0.147	0.0067
B	0.117	0.0123
C	0.102	0.0121
D	0.147	0.0067

Table 2 Mean and variance of feature points on the reflector antenna's side line before assembly (unit: cm)

Ideal x-coordinate	Value of t	Mean	Variance
0	0	0.1470	0.0067
18.3848	0.0884	0.1394	0.0044
36.7696	0.1788	0.1326	0.0037
55.1544	0.2714	0.1268	0.0036
73.5392	0.3664	0.1223	0.0036
91.9240	0.4639	0.1194	0.0036
110.3088	0.5643	0.1186	0.0036
128.6936	0.6678	0.1204	0.0036
147.0784	0.7746	0.1252	0.0036
165.4632	0.8852	0.1338	0.0041
183.8480	1.0000	0.1470	0.0067

The material of the reflector antenna is aluminum with Young's modulus E=69 GPa, and Poison's ratio v=0.35. The thickness of both parts is 1 mm. The sensitivity matrix $\boldsymbol{S}$ of all welding points is calculated by FEA in Abaqus® software. According to the arrangement of the reflector antenna's trusses, locating

points are determined in Abaqus® software before assembly, and deformations of the product after assembly are shown in Fig. 11.

As shown in Eq. (20), the deformations of feature points after assembly can be calculated using sensitivity matrix $\boldsymbol{S}$ and the sampled points in Table 2. The mean and variance of 11 feature points on the welding line in the y direction after assembly are obtained (Table 3).

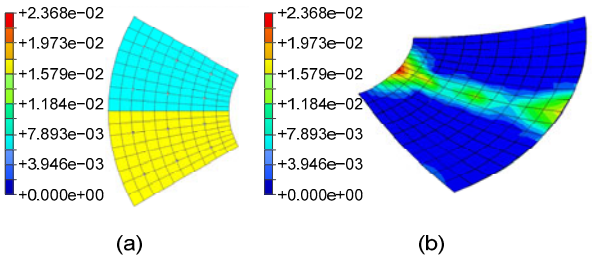

Fig. 11 Variation analysis of the reflector antenna in Abaqus®: (a) locating reflector antenna surfaces; (b) deformations of the welding line after assembly (References to color refer to the online version of this figure)

Table 3 Mean and variance of welding points on the reflector antenna's welding line after assembly (unit: cm)

Ideal x-coordinate	Value of t	Mean	Variance
0	0	0.0172	8.86×10^{-5}
18.3848	0.0884	0.0144	4.88×10^{-5}
36.7696	0.1788	0.0103	2.17×10^{-5}
55.1544	0.2714	0.0062	0.84×10^{-5}
73.5392	0.3664	0.0081	1.55×10^{-5}
91.9240	0.4639	0.0151	5.60×10^{-5}
110.3088	0.5643	0.0093	2.23×10^{-5}
128.6936	0.6678	0.0068	1.11×10^{-5}
147.0784	0.7746	0.0175	7.14×10^{-5}
165.4632	0.8852	0.0154	5.67×10^{-5}
183.8480	1.0000	0.0237	16.98×10^{-5}

Fig. 12 is the contrast of the interval of welding points after assembly and the allowed range of deviations, where the former is shown by the blue region and the latter is the range between the two red dotted lines. The result shows that the success rate of reflector antenna assembly in this situation is 96.5%.

4.2 Assembly of aircraft skins with a conformal array antenna

Another example is the assembly of aircraft skins that have a conformal array antenna. The goal is to calculate the line deformation (marked in red in Fig. 13), which will influence the function of the conformal array antenna.

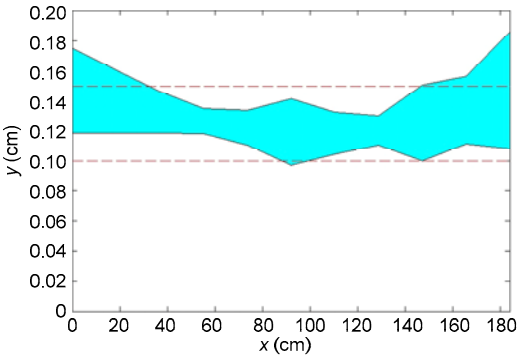

Fig. 12 Contrast of the interval of welding points after assembly and the allowed range of deviations (References to color refer to the online version of this figure)

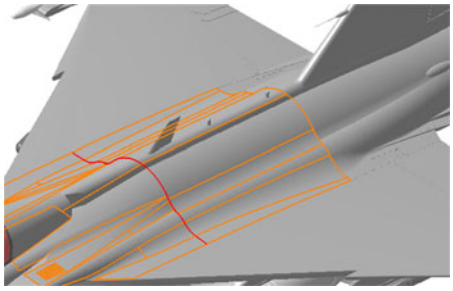

Fig. 13 Assembly of aircraft skins with a conformal array antenna (References to color refer to the online version of this figure)

Aircraft skin always needs to be modeled by high-order curve fitting because of its complex structure; here, we set n=6. The connecting direction of the side line's starting and ending points is treated as the x axis to build a coordinate system. A set of feature points on the side line are sampled as shown in Fig. 14, and some of their coordinates are (0, 0), (4.33, 0.151), (8.753, 1.93), (11.264, 3.271), (14.976, 5.666), (25.5, 10.711), (36.024, 5.666), (39.736, 3.271), (42.247, 1.93), (44.304, 0.652), (46.67, 0.151), and (51, 0) (in decimeters). Seven control point coordinates of the side line are calculated according to Section 2.3 as $\boldsymbol{A}$(0, 0), $\boldsymbol{B}$(10.38, 0.6), $\boldsymbol{C}$(15.56, −2.3), $\boldsymbol{D}$(25.5, 36.72), $\boldsymbol{E}$(35.44, −2.3), $\boldsymbol{F}$(40.62, 0.6), and $\boldsymbol{G}$(51, 0).

The fitting curve based on the sampling points is shown in Fig. 15, where the blue line connects control points, the red line is the fitting curve, and the red dots are some of the sampling points.

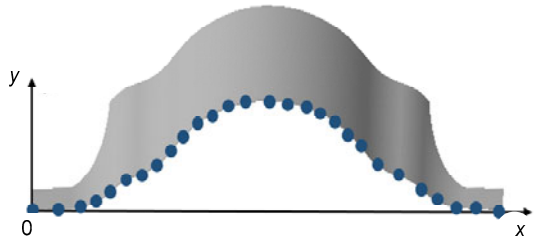

Fig. 14 Sampling points on the side line of aircraft skin

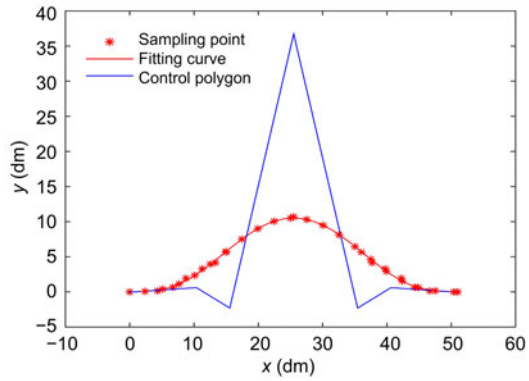

Fig. 15 The fitting curve based on sampling points (References to color refer to the online version of this figure)

In the design stage, the manufacturing tolerance of aircraft skin is set as 0.1 dm and its upper and lower deviations are +0.06 dm and −0.04 dm, respectively. Based on the equations mentioned in Section 2.3, the boundaries of seven control points are obtained according to the number of sampling points on the side line. Their limits are [−0.0057, 0.0086], [−0.0166, 0.0249], [−0.0415, 0.0622], [−0.0553, 0.0829], [−0.0415, 0.0622], [−0.0166, 0.0249], and [−0.0057, 0.0086] (in decimeters) in turn. These control points of the aircraft skin's side line have deviations from ideal positions in the y direction and all of them are supposed to follow a normal distribution. Their mean and variance values are shown in Table 4.

According to the method proposed in Section 2, the feature points on the side line are calculated. Their mean and variance are based on the value of t, which is in the interval [0, 1], and the actual shape of the aircraft skin's side line is illustrated in Fig. 16.

Sampling welding points in the region of the conformal array antenna and x values of 13 welding points are 15.1259, 16.8206, 18.5309, 20.2568, 21.9962, 23.7455, 25.5000, 27.2545, 29.0038, 30.7432, 32.4691, 34.1794, and 35.8741 (in decimeters) based on a ratio of chord lengths. Their mean and variance values in the y direction before assembly are shown in Table 5, as well as their corresponding t values in the Bernstein basis function.

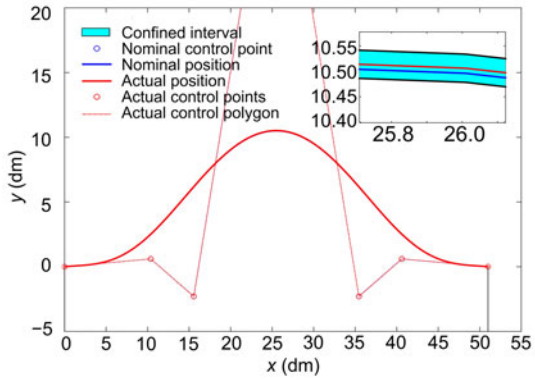

Fig. 16 Mean and variance distributions of feature points on the side line of the aircraft skin (References to color refer to the online version of this figure)

Table 4 Mean and variance of the aircraft skin's control points on the side line

Control point	Mean (dm)	Variance (dm)
A	0.0015	0.57×10^{-5}
B	0.0041	4.78×10^{-5}
C	0.0103	29.87×10^{-5}
D	0.0138	53.05×10^{-5}
E	0.0103	29.87×10^{-5}
F	0.0041	4.78×10^{-5}
G	0.0015	0.57×10^{-5}

Table 5 Mean and variance of feature points on the aircraft skin's side line before assembly (unit: dm)

Ideal x-coordinate	Value of t	Mean	Variance
15.1259	0.2930	0.0078	5.33×10^{-5}
16.8206	0.3275	0.0085	6.19×10^{-5}
18.5309	0.3620	0.0090	6.97×10^{-5}
20.2568	0.3965	0.0094	7.63×10^{-5}
21.9962	0.4310	0.0097	8.13×10^{-5}
23.7455	0.4655	0.0099	8.44×10^{-5}
25.5000	0.5000	0.0100	8.55×10^{-5}
27.2545	0.5345	0.0099	8.44×10^{-5}
29.0038	0.5690	0.0097	8.13×10^{-5}
30.7432	0.6035	0.0094	7.63×10^{-5}
32.4691	0.6380	0.0090	6.97×10^{-5}
34.1794	0.6725	0.0085	6.19×10^{-5}
35.8741	0.7070	0.0078	5.33×10^{-5}

The aircraft skin material is aluminum alloy with Young's modulus E=72 GPa and Poison's ratio v=0.33. Thickness of both parts is 5 mm. Sensitivity matrix $\boldsymbol{S}$ of all welding points is calculated by FEA in Abaqus® software. The gridding mesh of two assembled aircraft skin parts is shown in Fig. 17 and the deformations of the product in Fig. 18.

The mean and variance of 11 feature points on the welding line in the y direction after assembly are shown in Table 6.

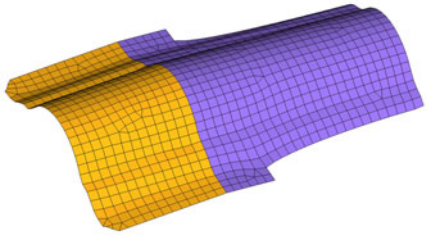

Fig. 17 Gridding mesh of aircraft skin assembly parts

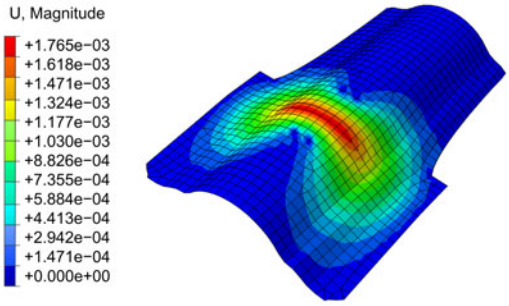

Fig. 18 Deformations of the aircraft skin welding line

Table 6 Mean and variance of welding points on the aircraft skin's welding line after assembly (unit: dm)

Ideal x-coordinate	Value of t	Mean	Variance
15.1259	0.2930	0.0078	5.33×10^{-5}
16.8206	0.3275	0.0085	6.19×10^{-5}
18.5309	0.3620	0.0090	6.97×10^{-5}
20.2568	0.3965	0.0094	7.63×10^{-5}
21.9962	0.4310	0.0097	8.13×10^{-5}
23.7455	0.4655	0.0099	8.44×10^{-5}
25.5000	0.5000	0.0100	8.55×10^{-5}
27.2545	0.5345	0.0099	8.44×10^{-5}
29.0038	0.5690	0.0097	8.13×10^{-5}
30.7432	0.6035	0.0094	7.63×10^{-5}
32.4691	0.6380	0.0090	6.97×10^{-5}
34.1794	0.6725	0.0085	6.19×10^{-5}
35.8741	0.7070	0.0078	5.33×10^{-5}

Under these tolerance design and assembly process conditions, the maximum deviation of feature points in the region of the conformal array antenna on the aircraft skin is (0.17±0.38) mm. These deviations can be regarded as inputs to calculate the influence of the electrical function caused by structure deformations.

5 Conclusions

Most existing variation analysis methods either neglect the relationships among neighboring points or regard the distributions of all feature points on surfaces as the same. In this paper, a kind of flexible curved surface assembly that can be simplified to the matching of side lines is considered based on Bézier curves to solve these two problems in antenna assembly. The distributions of feature points on side lines are obtained using control points. They are regarded as the inputs of FEA, and the deformations of final products are calculated. The quality of assembly is predicted according to the clearance of the mean position and the nominal position of the welding line, as well as the width of the confidence interval. Finally, the method is illustrated using two cases (reflector antenna surface assembly and aircraft skin assembly with a conformal array antenna) to show its feasibility.

In the future, we will consider the factors of surface splicing and the curved surface requirements that must be satisfied during the assembly process. For instance, the curvatures of corresponding welding points must be the same for assembly. The traditional finite element method used in variation analysis is limited because it must be repeated as welding points are changed. So, a new method that calculates the stiffness matrix according to structure and material properties will be considered.

References

Cai N, Qiao LH, 2011. Dimensional variation analysis of compliant sheet metal assembly. 2nd Int Conf on Digital Manufacturing and Automation, p.429-432. https://doi.org/10.1109/ICDMA.2011.112

Camelio JA, Hu SJ, Marin SP, 2004. Compliant assembly variation analysis using component geometric covariance. *J Manuf Sci Eng*, 126(2):355-360. https://doi.org/10.1115/1.1644553

Chaumette D, 2006. Technical evaluation report. Meeting on multifunctional structures/integration of sensors and antennas, p.T1-T10. https://doi.org/10.14339/RTO-MP-AVT-141

Choi W, Chung H, 2015. Variation simulation of compliant metal plate assemblies considering welding distortion. *J Manuf Sci Eng*, 137(3):031008. https://doi.org/10.1115/1.4029755

Gerbino S, Patalano S, Franciosa P, 2008. Statistical variation analysis of multi-station compliant assemblies based on sensitivity matrix. *Int J Comput Appl Technol*, 33(1): 12-23. https://doi.org/10.1504/IJCAT.2008.021881

Guo JK, Li BT, Liu ZG, et al., 2016. Integration of geometric variation and part deformation into variation propagation of 3-D assemblies. *Int J Prod Res*, 54(19):5708-5721. https://doi.org/10.1080/00207543.2016.1158881

Huang WZ, Liu JY, Chalivendra V, et al., 2014. Statistical modal analysis for variation characterization and application in manufacturing quality control. *IIE Trans*, 46(5): 497-511. https://doi.org/10.1080/0740817X.2013.814928

Lancaster HO, Seneta E, 2005. Chi-Square Distribution. John Wiley & Sons, New York, USA. https://doi.org/10.1002/0470011815.b2a15018

Liao XY, Wang GG, 2005a. Employing fractals and FEM for detailed variation analysis of non-rigid assemblies. *Int J Mach Tools Manuf*, 45(4-5):445-454. https://doi.org/10.1016/j.ijmachtools.2004.09.008

Liao XY, Wang GG, 2005b. Wavelets-based method for variation analysis of non-rigid assemblies. *Int J Mach Tools Manuf*, 45(14):1551-1559. https://doi.org/10.1016/j.ijmachtools.2005.03.001

Lindau B, Wärmefjord K, Lindkvist L, et al., 2014. Method for handling model growth in nonrigid variation simulation of sheet metal assemblies. *J Comput Inform Sci Eng*, 14(3):031004. https://doi.org/10.1115/1.4027149

Liu J, Jin JH, Shi JJ, 2010. State space modeling for 3-D variation propagation in rigid-body multistage assembly processes. *IEEE Trans Autom Sci Eng*, 7(2):274-290. https://doi.org/10.1109/TASE.2009.2012435

Liu SC, Hu SJ, 1997. Variation simulation for deformable sheet metal assemblies using finite element methods. *J Manuf Sci Eng*, 119(3):368-374. https://doi.org/10.1115/1.2831115

Marciniak Z, Duncan JL, Hu SJ, 2002. Mechanics of Sheet Metal Forming (2nd Ed.). Butterworth-Heinemann, Oxford, UK.

Qu XT, Li XN, Ma Q, et al., 2016. Variation propagation modeling for locating datum system design in multi-station assembly processes. *Int J Adv Manuf Technol*, 86(5-8):1357-1366. https://doi.org/10.1007/s00170-015-8275-8

Rocca P, Anselmi N, Massa A, 2014. Interval arithmetic for pattern tolerance analysis of parabolic reflectors. *IEEE Trans Antennas Propag*, 62(10):4952-4960. https://doi.org/10.1109/TAP.2014.2342758

Tonks MR, Chase KW, 2004. Covariance modeling method for use in compliant assembly tolerance analysis. Int Design Engineering Technical Conf and Computers and Information in Engineering Conf, p.49-55. https://doi.org/10.1115/DETC2004-57066

Yang Z, McWilliam S, Popov AA, et al., 2013. A probabilistic approach to variation propagation control for straight build in mechanical assembly. *Int J Adv Manuf Technol*, 64(5-8):1029-1047. https://doi.org/10.1007/s00170-012-4071-x

Yu KG, Yang ZH, 2015. Assembly variation modeling method research of compliant automobile body sheet metal parts using the finite element method. *Int J Automot Technol*, 16(1):51-56. https://doi.org/10.1007/s12239-015-0005-6